PCCP

Accepted Manuscript




ROYAL SOCIETY OF CHEMISTRY

www.rsc.org/pccp

# Water channel formation and ion transport in linear and branched lipid bilayers

Shihu Wang and Ronald G. Larson
Department of Chemical Engineering, University of Michigan
2300 Hayward Street, Ann Arbor, Michigan 48109-2136

**ABSTRACT**

Using molecular dynamics simulations, we studied the influence of methyl chain branching on transmembrane potential induced formation of water channels in lipid bilayers and ion transport. We compared the response of a bilayer lipid that has multiple methyl branches diphytanoylphosphatidylcholine (DPhPC) with its straight-chain counterpart dipalmitoylphosphatidylcholine (DPPC) to a transmembrane potential created by an imbalance in ionic charges across the membrane. We found that, compared to the straight-chain DPPC lipid bilayer membranes, branched DPhPC lipid membranes require a higher critical transmembrane potential to break down, followed by water channel formation, and transport of anions and cations through the pore. We demonstrated that the bulkiness of the added methyl branches leads to "barrel-stave" pores in DPhPC membranes which require a higher transmembrane potential to produce than the toroidal pores produced in the straight chain DPPC lipid bilayers. Our results provided a deeper understanding of the water channel formation and ion transport through lipid bilayer membrane and might help explain the increased resistance to charge-induced poration in organisms with membranes abundant in branched lipids.

## INTRODUCTION

The composition of a lipid bilayer - which depends dramatically on the organism or tissue - affects greatly its properties.[1–8] For example, in archaea and bacteria that can thrive in extreme environments, lipids usually have methyl branches in their tails.[9–11] Lipid bilayers composed of branched lipids have been found to exhibit high structural stability and low permeability to proton and other ionic and nonionic solutes, relative to those composed of linear lipids.[12–14] As another example, the acyl chain length and degree of saturation affects the elasticity and thickness of the lipid bilayers.[7] In addition, the lipids can differ in their head groups, architectures, net charge, and hydrogen bonding capability, and such differences alter the interactions between lipids bilayers and cholesterol, peptides and other biological molecules embedded in the bilayers.[2,7,8]

Here, we focus on the effect that methyl branches on the hydrophobic acyl chains have on the permeation of ions across the membrane. One of the commonly used branched lipids is the multiple-methyl branched diphytanoylphosphatidylcholine (DPhPC). As shown in Fig. 1a, DPhPC is composed of hydrocarbon tails with stable saturated bonds and multiple methyl groups presented at regular intervals along the acyl chains, which makes it a good candidate to study the effect of methyl branching in contrast with the widely studied linear dipalmitoylphosphatidylcholine (DPPC) lipid. It has been shown that the presence of the multiple methyl branches results in some unique structural and dynamic properties, as is evidenced by the different deuterium order parameters and electron density profiles, the lower lateral diffusion constants, and the higher structural stability relative to its linear counterpart DPPC, as determined by recent molecular dynamics simulations.[15–19] Due to its unique structural and dynamic properties, DPhPC has been extensively employed as an excellent model bilayer for electrophysiological measurements and for the study of the interaction between lipid bilayers and proteins, peptides and other biological molecules.[20–33] For example, DPhPC bilayers have been widely used as a reconstitution matrix for various channel-forming peptides and proteins, such as alamethicin,[8,20,21,26,28,30] gramicidin,[23,27,29] penetratin,[24] melittin,[25] and tetanus toxin.[22,32] Compared to linear lipids, the relative smaller areal ratio of the headgroup to the chains of DPhPC lipid indicates that the lipid bilayer can accommodate peptide, such as alamethicin, in the head group region until the peptide/lipid ratios exceed a threshold of ~1/40 which allows investigation of peptides both at the surface and inserted into the lipid bilayers.[34] Moreover, the high bilayer stability of DPhPC makes it possible to investigate various biological membrane processes, such as proton transport,[22,27] and to be used in nano-devices for biosenor applications.[12,35–37]

Ion permeation and small-molecule transport across lipid membranes are vital for many biological activities.[38–43] Certain proteins and peptides assist this process by creating specific channels that selectively regulate the permeability and stability of cell membranes.[41–43] In protein-free membranes, on the other hand, the ion permeation and transport of hydrophilic substances can also be achieved via the formation of transient nanometer-size water channels in the lipid membrane with the help of a transmembrane potential or mechanical stress.[44–54] The transmembrane potential can be induced by an external electrical field during the electroporation process. As shown by many previous studies, electroporation via an external electric field has found an increasing number of practical applications, including direct transfer of genes, nucleic acids, proteins and other biologically functional molecules into cells and electrofusion of cells or

electroinsertion of membrane proteins.[44–54] In the absence of an external electrical potential, the jump in ion concentration across the membrane of a living cell typically creates a potential difference across the lipid membrane.[55–57] In such a case, the bulk ionic solution usually remains electrically neutral, and the potential difference across the membrane arises from the charge imbalance in the neighborhood of the membrane-solution interface. In addition, the presence of other charged molecules, such as positive charged antimicrobial peptides,[41,58,59] also contributes to the transmembrane potential. It has been shown that when this transmembrane potential is large enough, it also induces the formation of transient water channels in the lipid bilayers [55–57] allowing the vital exchange of ions and other biological materials in and out of the cells.

While the formation of water channels has been demonstrated by many studies, the influence of lipid architecture and the regulation of the ion and peptide transport has been less studied. It is known that the formation of water channels usually involves substantial rearrangement of lipids around the channel [28,48,53,60–64] and thus is expected to be affected by the characteristics of lipids, such as lipid fluidity, and lateral packing density, which in turn are affected by lipid architecture. For example, the presence of methyl branches on the lipid acyl tails results in loosely packed lipid bilayers and reduced lateral diffusion.[15,16] While loosely packed lipids usually facilitate water penetration into the lipid bilayer, the slow lateral diffusion does not. To their surprise, O'Riordan and coworkers found in a recent study that listeria monocytogenes deficient in branched chain fatty acids is more susceptible to being killed by antimicrobial peptides than when there is no branched-lipid deficiency.[65] Since one of the antimicrobial mechanisms is pore formation in the membrane,[20,41,66] these results suggests a relative ease of water channel formation and less resistance to penetration and incorporation of antimicrobial peptides in densely packed linear lipids. To achieve a better understanding of the influence of methyl branches of acyl tails on the formation of water channels and to explain the differences in morphologies of water channels for branched and unbranched bilayers, here we use molecular dynamics simulations to study linear DPPC and methyl branched DPhPC lipid bilayers. We compare their ion permeabilities and water channel formation. Such results are expected to provide a deeper understanding of water channel formation and how it is influenced by lipid properties.

## SIMULATION DETAILS

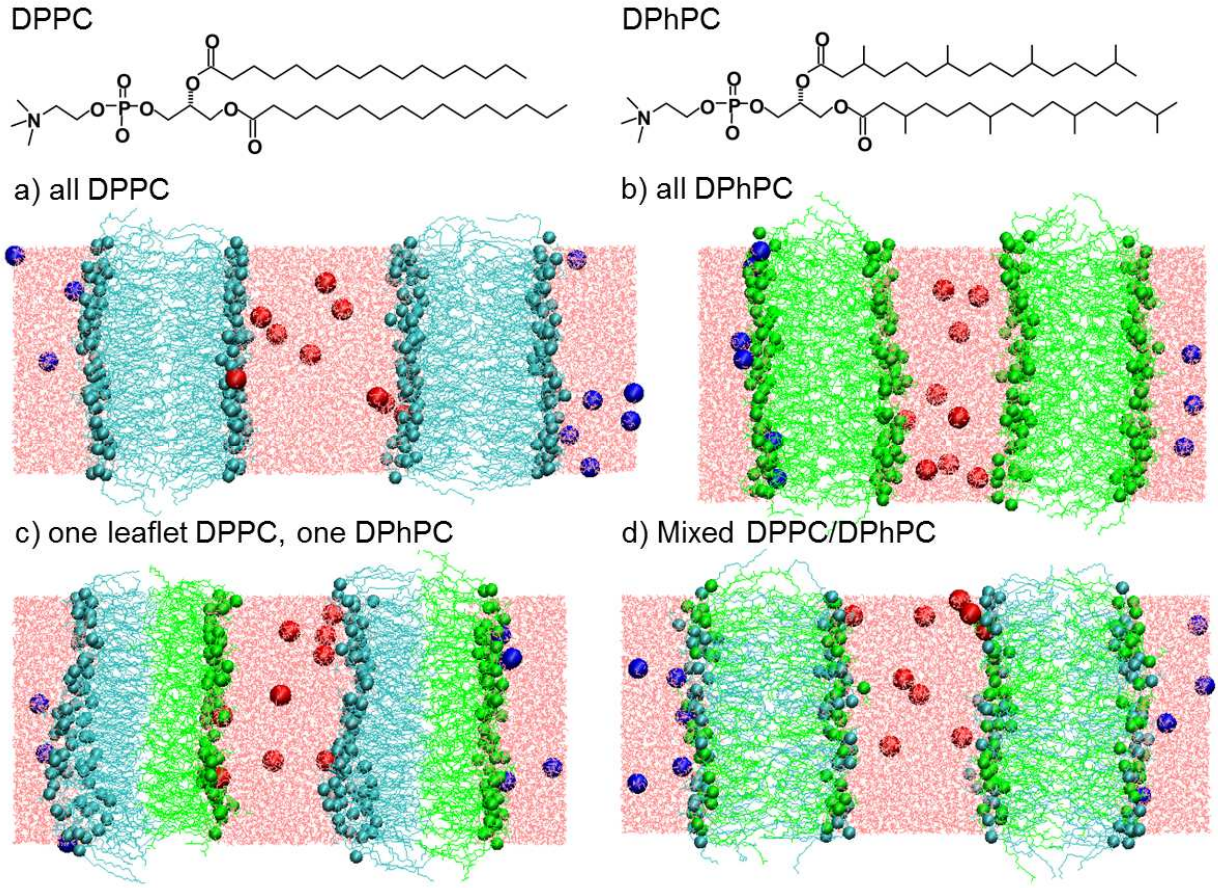


FIGURE 1 Chemical structures of DPPC and DPhPC and snapshots from different simulation set-ups: a) double DPPC lipid bilayers; b) double DPhPC lipid bilayers; c) one leaflet consisting of only DPPC lipids and the other of only DPhPC lipids; and d) each leaflet containing a mixture of DPPC and DPhPC lipids. In each setup, phosphorus atoms of lipids are shown as spheres, with cyan for DPPC and green for DPhPC. Cl- ions are shown as red and Na+ ions blue spheres. SPC/E water molecules are shown in pink.

We employ a double bilayer set-up to study the influence of methyl branching of lipid tails on the formation of a water channel in the lipid bilayers,[56,57] unless mentioned explicitly otherwise. Two different lipids are considered: linear dipalmitoylphosphatidylcholine (DPPC) and its multiple methyl-branched counterpart diphytanoylphosphatidylcholine (DPhPC). As shown in Fig. 1, we compare the following scenarios:

- Lipid bilayers consisting of 64 pure DPPC or DPhPC lipids in each leaflet. Each lipid bilayer has two leaflets, and two lipid bilayers are used to create the double bilayer setup. In total, there are 256 lipids in each system. (Fig. 1a&b)
- Lipid bilayers consisting of 64 DPhPC lipids in one leaflet and 82 DPPC lipids in the other leaflet of each bilayer. Two of these lipids bilayers are arranged with each DPPC leaflet facing a DPhPC one. The differing numbers of DPhPC vs. DPPC lipids per leaflet are chosen to make the surface areas per leaflet comparable (in the absence of ions) despite the difference in the bulkiness of the tails. (Fig. 1c) Since the ion concentration

in our simulation is rather low, corresponding to a salt concentration no higher than 0.060 M, based on previous findings[19,67], we do not expect the ions to affect the area per lipid very much (i.e., the area per lipid should change by much less than 2 Å$^2$).

- Lipid bilayers consisting of 32 DPPC and 32 DPhPC lipids mixed randomly in each leaflet. (Fig. 1d)

There are more than 11000 water molecules in each double bilayer system, i.e. around 38 water molecules/lipid when each leaflet is a mixture of different lipids, and 43 water molecules/lipid otherwise. These water molecules form two distinct water compartments that are separated by two bilayers. Each system is equilibrated for 20ns and then is used in the following electroporation study.

To model the transmembrane potential difference, several water molecules in one compartment, here called the "inner compartment", are replaced randomly by Cl-, and in the other, "outer compartment", are replaced by Na+ with one water molecule removed for each ion inserted. Equal numbers of ions are placed in the inner and outer compartments, varying from 1 to 15, to model different anion and cation concentrations and to produce different initial charge imbalances and thus different transmembrane potentials. Please note that the net initial charge imbalance across each of the two bilayers is the same as the number of ions in each water compartment. This is because the net charge difference is two unit charges per one ion pair and there are two bilayers in the system. Following the method described in Ref. [56], we calculate the potential profile of the lipid bilayers by twice integrating the charge density along the bilayer normal and then averaging the output over both lipid bilayers. We find that a simulation with a charge imbalance of 1e created a transmembrane potential of approximately 400mV. This is similar to a result found in an earlier study,[56] which also showed that the transmembrane potential is directly proportional to the charge imbalance. We further note that the ion concentration, and thus the transmembrane potential, is fairly large in order to simulate pore formation within the time scale that is achievable by molecular dynamics simulations. A lower ion concentration produces a smaller transmembrane potential but requires a much longer time to observe the poration in lipid bilayer.[44,56] An example snapshot of the initial setup with 9 Na+ in one compartment and 9 Cl- in the other is shown in Fig 1. We perform 50ns simulation for each system containing different concentrations of ions.

The GROMACS 4.5.4 suite [68,69] with Gromos G53a6 force field [70] is used for all the simulations in this study. The structure for DPPC is downloaded from the GROMACS website and DPhPC from lipidbook.[71] The SPC/E water model and the default ion parameters in the GROMACS force field are used. All simulations are performed in an NPT ensemble at the physiological temperature of 310K or a higher temperature of 323K by coupling the lipids and the rest of the system separately to a Berendsen thermostat with a coupling constant of 0.1 ps. Although some previous molecular dynamics simulations involving DPPC lipids have been performed at 323K to make sure that the DPPC membrane is well above its phase transition temperature, most of our simulations are carried out at 310K for the following reasons: a) most experimental studies on DPhPC were not performed at a temperature as high as 323K; b) 310K is the physiological temperature, which is slightly above that for the phase transition of the DPPC bilayers determined in simulations, i.e., 305K;[72] c) Most importantly, the lateral diffusion coefficient of linear DPPC lipids is closer to that of branched DPhPC lipids at 310K than at it is at 323K, as

discussed below. This allows us to minimize the influence of the lateral diffusion and demonstrate the importance of the steric effects of chain branching on the morphologies of water channels. The pressure is semi-isotropically coupled to a barostat at 1 atm pressure with a coupling constant of 1ps. A cutoff of 1.2 nm is used for the short-range interactions. The long-range electrostatic interactions are calculated using the particle mesh Ewald algorithm with tin-foil boundary conditions. All bonds are constrained using the LINCS algorithm. Simulations are saved every 10 picoseconds for subsequent analysis.

## RESULTS AND DISCUSSIONS

### Properties of Field-Free Lipid Bilayers

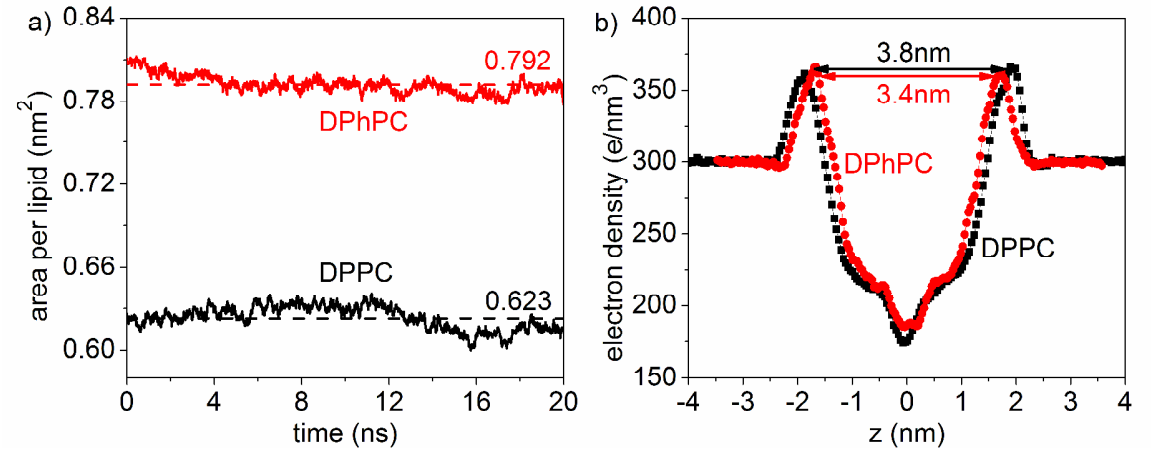


FIGURE 2 a) Area per lipid as a function of time and b) electron density as a function of bilayer normal z for linear DPPC lipids and branched DPhPC lipids. The temperature is 310K.

We first consider the properties of the lipid bilayers in the absence of a transmembrane potential. Plotted in Fig. 2a is the area per lipid as a function of simulation time at T=310K for both DPPC and DPhPC membranes. The average area per lipids over 20ns simulation from Fig. 2a is 0.623 nm$^2$ for linear DPPC lipid bilayers and 0.792nm$^2$ for branched DPhPC, both of which are close to those obtained from previous molecular dynamics studies.[15,72] The thickness of the lipid bilayer, indicated in Fig. 2b by the peak-to-peak distance in the electron density profile along the bilayer normal, is slightly smaller for DPhPC than for DPPC lipid bilayers (3.4nm for DPhPC vs. 3.8nm for DPPC). We find that the thickness of DPPC lipid bilayers is the same as a previous study but that of DPhPC lipid bilayers is somewhat smaller (3.8nm vs. 3.4nm in this study).[16] Compared to the linear DPPC lipids, the larger area per lipid of DPhPC is due to the steric effects of multiple methyl branches of the latter. The results imply that the linear DPPC lipids are more tightly packed in the lipid bilayer, which might cause a slightly larger peak-to-peak distance than in branched DPhPC lipid bilayers.

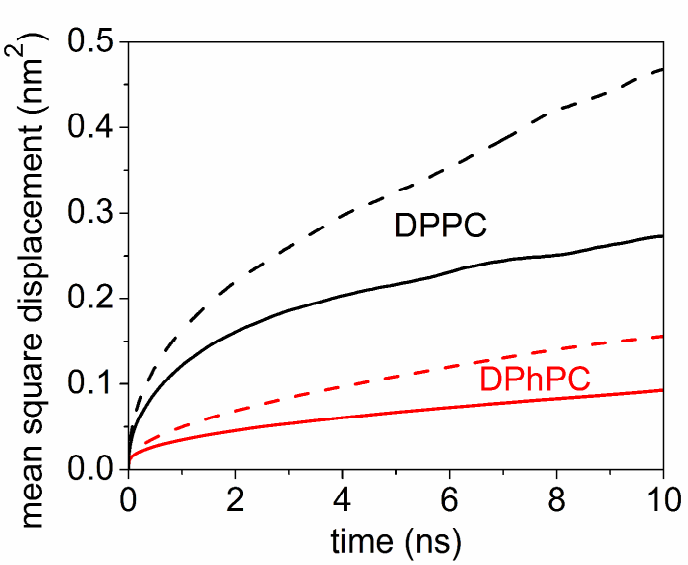


FIGURE 3 Mean-square displacement of lipid center of mass in the membrane plane at T=310K (solid lines) and T=323K (dashed lines).

Shown in Fig. 3 is the lateral mean square displacement of the center of mass of lipid molecules (perpendicular to the bilayer normal) as a function of time for both linear DPPC and branched DPhPC lipids at T=310K and T=323K. As is seen, similar to some previous studies, the mean square displacement is linearly proportional to time above 2ns.[73] The lateral diffusion coefficient, D, of the lipids is calculated from the mean square displacement of lipids versus time from the relations: $D = \lim_{t\to\infty} \frac{\left\langle \left| r(t-t_0) - r(t_0) \right|^2 \right\rangle}{4t}$, where r is the planar vector for the center of mass of a lipid molecule perpendicular to lipid bilayer normal. For linear DPPC lipids, this result in a diffusion coefficient of D=1.66×10$^{-8}$cm$^2$/s at T=310K and D=7.80×10$^{-8}$cm$^2$/s at T=323K and for branched DPhPC lipids, D= 1.29×10$^{-8}$cm$^2$/s at T=310K and D=2.4×10$^{-8}$cm$^2$/s at T=323K. The results at T=323K are similar to those reported elsewhere at the same temperature.[73–75] We note that temperature has a larger relative effect on the lateral diffusivity of linear DPPC than of branched DPhPC lipids. The difference between the linear and branched DPPC lipids at 310K is much smaller than at 323K where the difference is a factor of three. A high lateral diffusivity implies that the linear DPPC lipids can rearrange themselves more rapidly under a transmembrane potential to allow the water molecules to penetrate the lipid bilayer more easily, as discussed below. To minimize the influence of the lateral dynamics of lipids on the water channel formation, we use a temperature of T=310K in most of our simulations.

If other lipid properties are the same, tightly packed and thicker lipid bilayers are usually thought to be more resistant to electroporation than loosely packed and thinner lipid bilayers. However, the presence of methyl branches also slows down the lipid lateral dynamics and affects the lipids properties differently as discussed above. As a result, the collective effect of methyl branches on water channel formation in lipids bilayer is complex to estimate priori.

**Water Channel Formation**

Before comparing electroporation in DPPC lipid bilayers with that in DPhPC, we illustrate, in this section, the formation of a water channel and ion transport through DPPC lipid bilayers at T=310K. In our simulations, the charge imbalance between inner and outer water compartment induces a transmembrane potential across each bilayer. As discussed in previous studies,[56,57] such a transmembrane potential aligns the dipoles of the water molecules along the transmembrane potential gradient, especially near the head group region of the lipid leaflets.

At modest charge imbalance, some water molecules penetrate slightly into the hydrophobic core of the lipid bilayer. When the charge imbalance is large enough (as discussed below, for DPPC, larger or equal to 8e; and for DPhPC, larger or equal to 11e), some water molecules in one compartment penetrate deeply and reach the other water compartment, resulting in the formation of a water channel across one of the lipid bilayers.

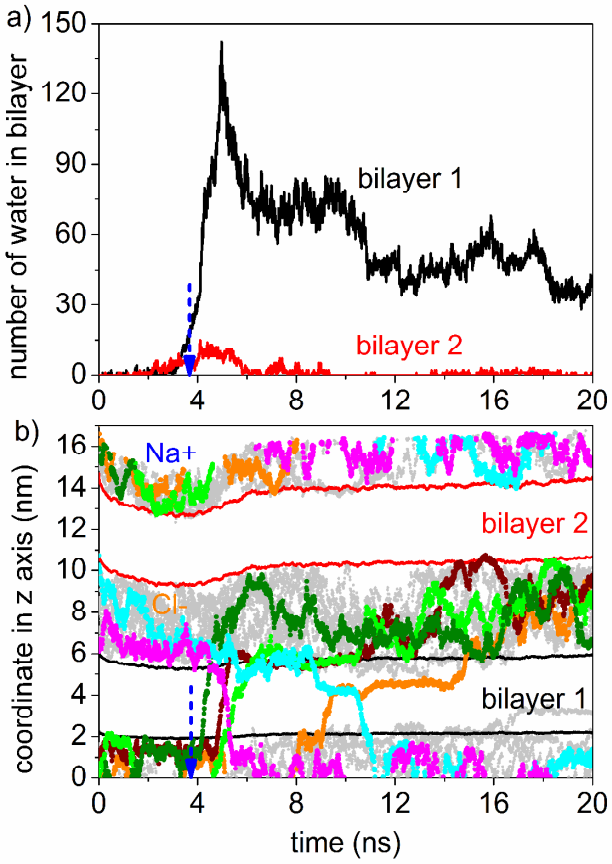


FIGURE 4 a) Number of water molecules within 0.8 nm of the center of each DPPC lipid bilayer and b) the z coordinates along the bilayer normal of all the cations and anions and the average z coordinates of phosphorus atoms on lipids as a function of time. For clarity, the translocating ions are shown in different colors and the ions that do not translocate within 30ns are shown in gray. The z coordinates of phosphorus atoms on the lipids of bilayer 1 are shown as black lines and that of bilayer 2 as red lines. The blue dashed arrow points to the simulation time at which the water channel forms in lipid bilayer 1. The lipid bilayers shown are composed of straight-chain DPPC lipids with each water compartment containing 9 ions at the beginning of simulation.

The process of the water channel formation inside a lipid bilayer is clearly seen in the Fig. 4a, where the number of water molecules inside each lipid bilayer is plotted as a function of time for double DPPC lipid bilayers with 9 Na+ ions in one water compartment and 9 Cl- ions in the other compartment initially. In this plot, the water molecules within 0.8nm of the center of mass of each lipid bilayer along the z direction, which is the bilayer normal, are taken to be inside the lipid bilayer. As shown in Fig. 4a, at the beginning of the simulation, there are no water molecules inside either lipid bilayer. As the simulation progresses, the number of water molecules increases in both lipid bilayers almost equally. At t=3.7ns, the number of water molecules inside bilayer 1 increases sharply, reaching a maximum within a few hundred picoseconds. Such a dramatic increase corresponds to the formation of a water channel in the lipid bilayer. After the number of water molecules inside the lipid bilayer reaches its maximum, it then decreases. We note that the number of water molecules in the other lipid bilayers increases only slightly from zero and then drops again to almost zero after the water channel forms in the other lipid bilayer.

In Fig. 4b, the z coordinates of the ions and the average z position of the phosphorus atoms in the each lipid leaflet are plotted as a function of simulation time. The average positions of the phosphorus atoms mark the boundaries of the lipid bilayers and water compartments. It can be seen that ions move randomly in each water compartment at the beginning of the simulation, but once the water pore forms, both anions and cations transport through the pore very quickly. The translocation of ions through the membrane reduces the charge imbalance across the lipid bilayer and thus leads to the shrinkage of the water channel. The behavior is similar for different initial charge imbalances (as long as they are as large or larger than 8e for DPPC and 11e for DPhPC), except for differences between DPPC and DPhPC described next.

**Critical Charge Imbalance**

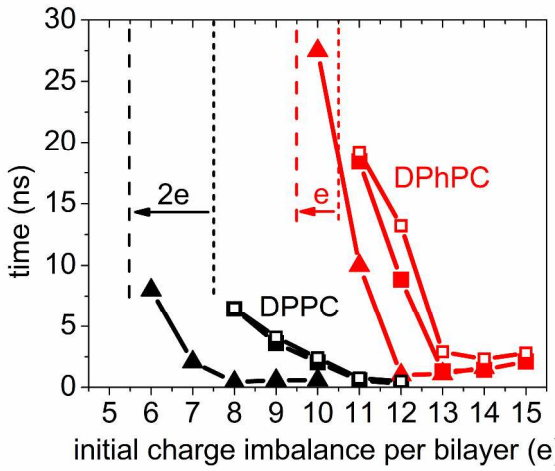


FIGURE 5 Time required for 15 water molecules to penetrate a lipid bilayer (solid squares: T=310K; solid upper triangles: T=323K), which marks the initiation of a water channel, and time for the first ion to translocate through the lipid bilayer (open symbols: T=310K), as a function of initial charge imbalance per bilayer. Dashed lines separate the "low" initial charge imbalance below which no water channel forms within 50ns from the "high" initial charge imbalance above which a water channel forms within 50 ns, where the short dashes are for 310K and the long dashes for 323K.

To compare the stability of different lipid bilayers against electroporation, we determine two critical simulation times: 1) for 15 water molecules to penetrate into the lipid bilayer triggering a rapid subsequent increase to a maximum and 2) for the first ion to translocate across a lipid bilayer. The former corresponds to formation of a channel in one of the lipid bilayers. We note that the critical time for channel formation depends on the initial charge imbalance, as shown in Fig. 5. As is seen, the formation of a water pore requires a certain initial charge imbalance, below which there is no water channel formation within 50ns of simulation. This observation is also qualitatively similar to previous findings that there exists a critical breakdown potential for the lipid bilayers to be electroporated.[47,48] Note that the breakdown potential is usually system specific, depending, for example, on lipid type, strength and frequency of the applied electrical fields, etc.[47,48] From Fig. 5, an increase in the initial charge imbalance above the critical value leads to fast formation of water channels. After the water channel forms, the first ions translocate through the lipid bilayers almost immediately. More interestingly, we find that lipid bilayers composed of branched lipid bilayers require a higher initial charge imbalance, i.e. 11e, than for a linear lipid, i.e. 8e, for a channel to form within 50ns. Above the critical charge imbalance, the water channels also form more quickly in the linear DPPC lipid bilayers than in the DPhPC lipid bilayers. This indicates that compared to linear DPPC lipid bilayers, the branched DPhPC lipids are more stable and resistant to electroporation even though they are less tightly packed in the bilayer. This conclusion also agrees with some experimental studies showing that branched lipids exhibit high salt-tolerance and electrical stability.[9,10,12,48,76]

To check the role of diffusivity, we also perform simulations at T=323K and calculated the critical time for the formation of water channels inside the lipid bilayers. We note from previous discussion that with increasing temperature, the lateral diffusion for both lipids increases, and the lateral diffusion of linear DPPC lipids is almost three times larger than that of branched DPhPC lipids at T=323K. As seen in Fig. 5, increasing temperature shifts the critical time to smaller values for both linear DPPC and DPhPC lipids. This is mainly due to the faster dynamics of lipid molecules at high temperature T=323K. Furthermore, we also observe a shift of the critical initial charge imbalance from 8e to 6e for DPPC bilayers, which is larger than the shift seen for DPhPC bilayers, from 11e to 10e. This implies that besides the difference in the water channel morphologies discussed below, the slow lateral diffusion of the branched lipids may be another factor responsible for the increased resistance of the DPhPC lipid bilayers to electroporation. It is important to point out here that even though the following discussions are based on results at T=310K, the conclusions, such as the difference in the pore morphologies between different lipids types, also qualitatively hold at T=323K.

**Pore Morphologies**

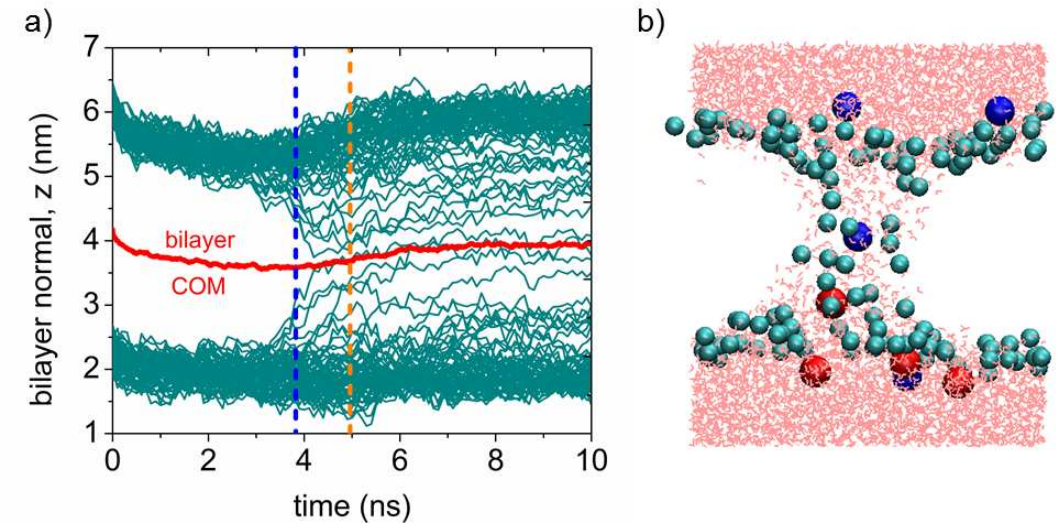


FIGURE 6 a) Z coordinates along the bilayer normal (cyan) of all phosphorus atoms of a DPPC lipid bilayer that forms a water channel and the center of mass (red) of this lipid bilayer as a function of time. The blue dashed line corresponds to the critical time when the water channel forms and the orange dashed line to the time when the number of water molecules inside the lipid bilayer reaches its maximum. b) Simulation snapshot taken at t=4.96ns when the number of water molecules inside the lipid bilayer reaches a maximum, i.e. corresponding to the orange dashed line in a). Each water compartment initially contains 9 ions. Na+ and Cl- ions, if present, are shown as blue and Cl- as red spheres, respectively. Water molecules are shown in pink. For clarity, only the phosphorus atoms on the lipids are shown (as cyan spheres).

In Fig. 6a, we plot the z coordinates of all the phosphorus atoms of the DPPC lipids as a function of time for the lipid bilayers that form a water channel. As can be seen, initially all the phosphorus atoms in the two different leaflets are quite separated and are located at around 2nm and 5.5nm. The phosphorus atoms in each leaflet retain the same z value until the water channel starts to form at 3.7ns. During the water channel formation, the number of water molecules inside the lipid bilayer increases quickly as seen in Fig. 4a. We also observe a reorganization of lipids in the vicinity of the water channel with the lipid heads entering into the lipid bilayer and moving closer to the center of mass of the lipid bilayer as shown in Fig. 6a. This collective reorganization of the lipids occurs almost simultaneously with the formation of the water channel. From the snapshot at time t=4.96ns when the number of water molecules reaches a maximum of 117, we observe in Fig. 6b that the linear DPPC lipid molecules no longer form a planar lipid bilayer and some of their headgroups enter the water channel, with their lipid tails pressed into the region occupied by neighboring lipids. The lipid heads line up along the edge of the pore, which forms a curved interface between the waters and the lipid tails. Similar hydrophilic pores have also been reported by Marrink and coworker at T=323K.[51] We find that the structure of this water channel is quite similar to the toroidal model proposed by Matsuzaki [77] and Ludtke [78] to describe pores induced by the anti-microbial peptide Magainin, but in our case, of course there is no peptide present.

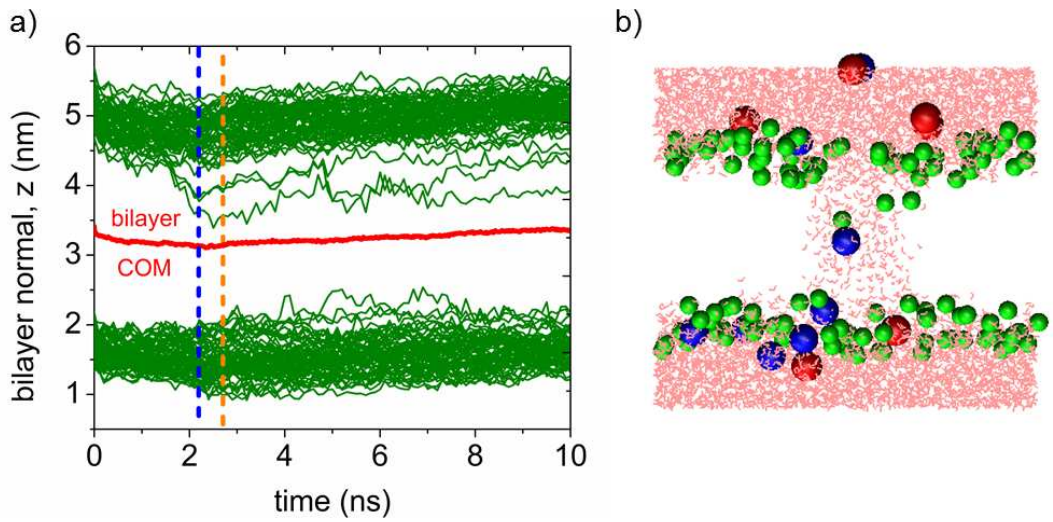


FIGURE 7 a) The same as in Fig. 6, except for a DPhPC lipid bilayer shown in green b) Simulation snapshot taken at t=2.70ns when the number of water molecules inside the lipid bilayer reaches maximum, i.e. at time corresponds to the orange dashed line in a). Each water compartment contains 14 ions at the beginning of the simulation. For clarity, only the phosphorus atoms on the lipids are shown (as green spheres).

For comparison, the z coordinates of all the phosphorus atoms of the branched DPhPC lipid bilayer as a function of time are shown in Fig. 7a for an initial charge imbalance of 14e. Note that an initial charge imbalance of 11e is required for the formation of a water channel in the branched DPhPC lipid bialyers within 50ns, while for linear DPPC lipids only a charge imbalance of 8e is required. However, as can be seen, during the formation of the water channel inside the branched DPhPC lipid bilayer, only a very few lipids (i.e. 3 lipids) reorganize and move towards the lipids bilayer center of mass even with an initial charge imbalance of 14e. From the snapshot taken at time t=2.70ns when the number of water molecules in the lipid bilayer reaches a maximum of 149 in Fig. 7b, we find that the morphology of the water channel in DPhPC is quite different from that for DPPC described above. Due to the steric effect from the multiple methyl branches, the branched DPhPC lipid tails groups are much bulkier than those of the linear DPPC lipids. As a result, it is apparently hard for DPhPC tails to bend as much as the linear DPPC tails do to allow the hydrophilic head groups to move inside the hydrophobic core of the lipid bilayer. Instead, we observe that only a few branched DPPC lipids move away from their original planar bilayer structures. The water channel, therefore, is surrounded mostly by the hydrophobic branched lipids tail groups with little channel curvature. The DPhPC channel has a cylindrical shape that is more consistent with the barrel-stave model[79] than the toroidal pore model.[77,78]

**Implications of Water Channel Morphologies**

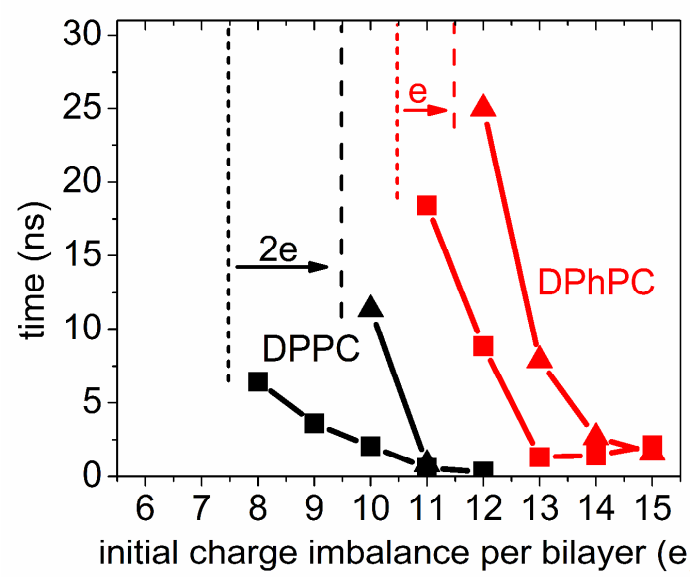


FIGURE 8 Time at which 15 water molecules penetrate the lipid bilayer, initiating formation of a water channel, as a function of initial charge imbalance per bilayer. Square symbols are from the original simulation with no constraints applied, as in Fig. 5. The simulation results with constraints applied are shown as upper triangles. Dashed lines separate the region of low initial charge imbalance where no water channel forms within 50ns from the region of high initial charge imbalance where the water channel forms within 50 ns.

The difference in the water channel morphologies has a number of implications. Firstly, even though formation of a hydrophilic toroidal water channel in DPPC lipid bilayers involves a large rearrangement of lipids, it forms at lower field than does the hydrophobic barrel-stave channel in branched DPhPC lipid bilayers. To prove this point, we carry out the following simulation: we apply position restraints on the phosphorus atoms in the lipid heads and restrict their movement along the lipid bilayer normal. This constraint prevents even the linear DPPC lipids from bending to enter the hydrophobic core of the lipid bilayer, and forming toroidal water channels. We perform the same calculations as discussed above and determine the critical charge imbalance required to form the water channel inside lipid bilayer. As is seen in Fig. 8, with this constraint, the critical initial charge imbalance required for water channel formation inside linear DPPC lipid bilayer increases from 8e to 10e, much closer to that of branched DPhPC lipid bilayers. On the other hand, with this constraint the critical charge imbalance for DPhPC lipid bilayer changes less, shifting only from 11e to 12e. This indicates that by prohibiting the formation of a hydrophilic toroidal water channel and favoring the formation of barrel-stave water channels, a larger initial charge imbalance is required to form a water channel. This implies that the toroidal pore is easier to form than the barrel-stave pore, even though the former involves greater lipid rearrangement. A likely explanation is that the hydrophilic head-group lining of the toroidal pore minimizes direct contact between water and lipid tails, which is unavoidable in the more unstable hydrophobic barrel stave pores.

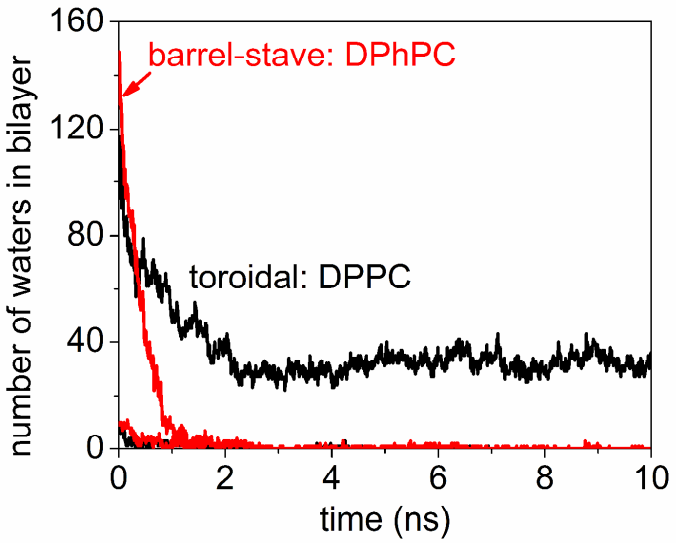


FIGURE 9 Number of water molecules inside lipid bilayers as a function of time after removal of the charge imbalance across the membrane used to form a channel. Data for linear DPPC lipid bilayers forming toroidal water channels are shown in black and for branched DPhPC lipid bilayers forming barrel-stave water channels in red lines. Each system has two lines representing the two lipid bilayers in the double bilayer setup.

Secondly, once formed, the hydrophilic toroidal water channels inside the DPPC lipid bilayers are more stable that those of the hydrophobic barrel-stave water channels inside the DPhPC lipid bilayers. We find that after its reaches a maximum, the number of water molecules inside the branched DPhPC lipid bilayers drops much more quickly than that inside the linear DPPC lipid bilayers. To further validate this point, we select for further study the following conformations of lipid bilayers with water channels from previous simulations: linear DPPC lipid bilayers with 9e initial charge balance at t=4.96ns and branched DPhPC with 14e initial charge imbalance at t=2.70ns. We note at these times both simulations had already formed water channels inside one of the lipid bilayers: there are 117 water molecules inside one of the DPPC lipid bilayers and 149 water molecules inside one of the DPhPC lipid bilayers. At this point in each simulation, we then remove the ions to eliminate the transmembrane potentials and performed 10ns molecular dynamics simulations with otherwise the same conditions as before. The numbers of water molecules inside lipid bilayers are calculated and plotted in Fig. 9 as a function of time. It is not surprising to find that the hydrophobic barrel-stave water channel inside the branched DPhPC lipid bilayer shrinks much faster and disappears within 2 ns, while the toroidal water channel inside the linear DPPC lipid bilayer still retains 32 water molecules even after 10ns.

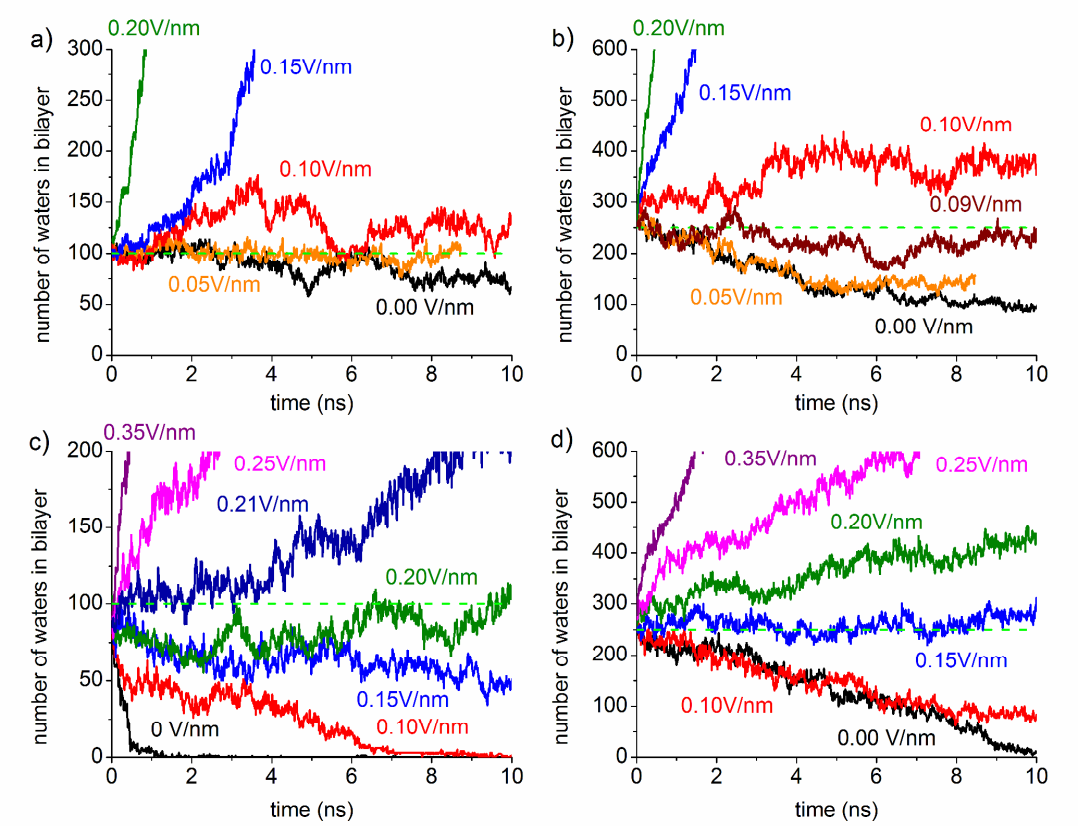


FIGURE 10 Number of water molecules inside lipid bilayers as a function of time when different external electric fields are applied to the torodial water channels of pore sizes a) 100 and b) 250 water molecules and barrel-stave water channels of pore size c) 100 and d) 250 water molecules. The horizontal dashed lines correspond to the number of water (either 100 or 250) inside the original pore.

To further check the stability of water channels, we also perform simulations with a single bilayer setup and applied external electric fields across the lipid bilayer. To account for large pore sizes, the single lipid bilayer consists of 160 lipids with 80 lipids per leaflet and 9100 water molecules in each simulation box. All other simulation conditions are kept the same as the double bilayer setup. Please note in this case, no implicit ions are used, and the transmembrane potential is implemented by maintaining a fixed voltage difference corresponding to a field strength of E with units of V/nm across the lipid bilayer by adding a force of $F=q_iE$ on all the atoms carrying a charge $q_i$ [80]. Different sizes of toroidal water channels in the DPPC lipid bilayers and barrel-stave pores in the DPhPC lipid bilayer are examined.

In Fig. 10, the number of water molecules inside the lipid bilayer as a function of time is plotted for different external electric fields. As is seen in Fig. 10a, for small water channel with 100 water molecules, the toroidal water channel inside the bilayer composed of linear DPPC lipids are rather stable under low electric fields, i.e. E<=0.05V/nm. The number of water molecules in the bilayer only decreases slightly within 10ns even when no external electric field is applied. As discussed above, this is due to the fact that collapse of the toroidal water channel to form a perfect bilayer requires large-scale lipid rearrangement, which takes a long time. When the

electric field increases above 0.10V/nm, the number of waters in the bilayer increases somewhat and instead fluctuates in time. When the electric field is around 0.15V/nm, the number of waters inside the torodial water channel increases quickly leading to the rupture of lipid bilayer within a very short time. The critical electric field separating slow pore shrinkage from rapid expansion is around 0.10 V/nm for a toroidal pore of this initial size.

On the other hand, the small barrel-stave water channel in Fig. 10c shrinks and finally disappears when no electric field or small electric fields are applied across the lipid bilayer. Even with field strength of 0.10V/nm, the barrel-stave channel collapses and the bilayer is pore-free within 10ns of simulation. The barrel-stave water channel can only sustain its size under a rather large external electric field around 0.20V/nm. A slight increase of the electric field above 0.20V/nm leads to a quick increase in the number of water in the bilayer and finally the rupture of the bilayer. Compared to toroidal water channel, we find that the barrel-stave water channel is much more unstable and requires a larger external electric field to be maintained.

For large toroidal water channels with 250 water molecules in the bilayer in Fig. 10b, the number of waters inside the channel decreases slowly under low electric fields. We also note that the channel never disappears even after 40ns of simulation. Compared to small toroidal water channels in Fig. 10a, a rather similar strength of electric field around 0.09V/nm is required to sustain the large toroidal water channel. For the barrel-stave channel of similar size in Fig. 10d, we find that an electric field around 0.15V/nm is required to sustain the channel. The electric field required to sustain for large-size channels is smaller than that for smaller channels because of the increase in the number of polarizable waters inside the water channel.

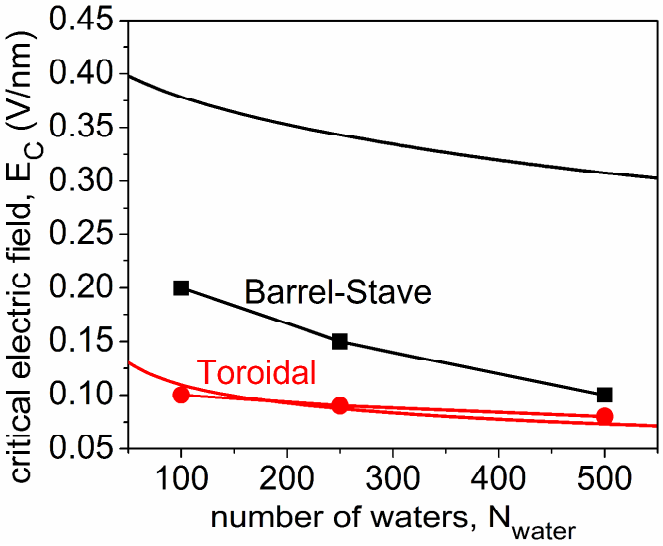


FIGURE 11 Critical electric field, $E_C$, to hold water open channels as a function of the number of waters inside the water channel. Symbols, connected by lines are from the simulations, and the solid lines are theoretical predictions.

We summarize our finding of pore stability in Fig. 11, where the critical electric field as a function of number of waters is shown for the barrel-stave and toroidal pores. From our simulations we observe several points: a) once formed, toroidal water channels require a smaller

critical electrical field to sustain than do barrel-stave water channels. Below its critical electric field, a toroidal water channel is more stable than is barrel-stave channel due to the large re-arrangement of lipids required to break the toroidal water channel. When the electric fields is above the critical electric field, the lipid bilayers for both types of water channel rupture very quickly; b) for the range of water channels considered in our simulation, the critical electric fields needed to sustain the water channel decreases with its size. This dependence on the size of the water channels is stronger in the barrel-stave pores; c) for large size pores, the critical electric fields for both toroidal and barrel-stave water channels are rather close to each other.

There have been many different models put forward to explain electroporation[48,49]. We have adapted one of the theoretical models (detailed derivation shown in the Appendix) and compared its predictions with our simulation results in Fig. 11. As is seen, there is a fairly good agreement between the simulation results and theoretical predictions for the toroidal water channels. However, for the barrel-stave pore, even though the predicted dependence of the critical electric field on pore size, i.e., number of waters inside the channel, is qualitatively similar to the simulated one, the critical electric field from the theoretical model is three times than is obtained from the simulations.

Lastly, we want to point out that the fundamental difference in the pore formation and morphologies between the linear and branched lipid bilayers is also biologically significant. For example, the toroidal pore in the linear lipid bilayers disrupts the lipid bilayers by reorganizing the hydrophobic and hydrophilic parts of the membrane. This is expected to facilitate greatly the transport of hydrophilic compounds across the lipid bilayers. The barrel stave water channel, on the other hand, disrupts the lipid bilayers, opens up the hydrocarbon core and provides a template for the self-assembly of some amphipathic peptides.[43] Additionally, the barrel-stave pores, as is seen in DPhPC lipid bilayers, form without significant distortion of the lipid bilayers and thus might be explained by a simple model that considers only surface energy contributions and ignores contributions from rearrangements of the lipid molecules.[81] Such a simple model of barrel-stave pores is also helpful for the development of a theoretical understanding for more complicated toroidal pores whose formation is usually accompanied by the lateral thermal fluctuation of lipid molecules and spontaneous formation of very small hydrophobic pre-pores.[44,81]

**Mixed Lipids**

In biology, lipid bilayers usually consist of a mixture of different lipid types. In certain cases, there is an asymmetric distribution of lipids across the membranes, which is considered to be important for many physiochemical properties of the biological membranes. To show how a mixture of linear and branched lipids and membrane asymmetry affect the water channel formation inside the lipid bilayers, we have also considered a couple of alternative lipid compositions described below.

For the first scenario, one leaflet of the lipid bilayer is composed of 82 linear DPPC and the other leaflet of 64 branched DPhPC lipids, as shown in Fig 1c. Those two leaflets make up one single lipid bilayer. By varying the initial charge imbalance, we calculate the critical charge imbalance/critical simulation time when the water channel forms in one of the lipid bilayers. We find that the formation of the water channel within 50ns in this mixed leaflet situation requires a

charge imbalance of 10e, which is higher than 8e for pure linear DPPC lipid bilayers but lower than 11e for pure branched DPhPC lipid bilayers.

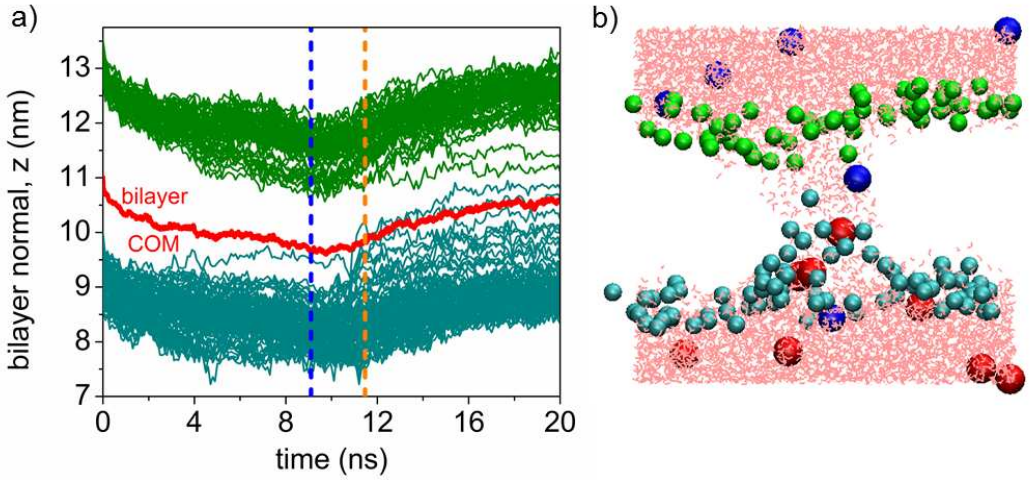


FIGURE 12 a) Z coordinates along the bilayer normal (cyan lines for DPPC and green lines for DPhPC) of all the phosphorus atoms of the lipid bilayer that form water channels and the center of mass (red) of this lipid bilayer as a function of time. The blue dashed line corresponds to the critical time when the water channel forms and the orange dashed line to the time when the number of water molecules inside the lipid bilayer reaches its maximum; b) Simulation snapshot taken at t=11.47ns when the number of water molecules inside the lipid bilayer reaches a maximum, i.e. at time corresponding to the orange dashed line in a). The lipid bilayers are composed of one leaflet of branched DPPC lipids and one branched DPhPC with each water compartment containing 11 ions at the beginning of simulation. Na+ ions, if present, are shown as blue and Cl- as red spheres, respectively. Water molecules are shown in pink. For clarity, only the phosphorus atoms on DPPC are shown as cyan spheres and DPhPC as green spheres.

If the charge imbalance is above 8e but below 10e, we find that the leaflet composed of linear DPPC lipids is usually disrupted. However, the charge imbalance is not high enough to induce water channel formation in the other leaflet composed of branched DPhPC lipids. As a result, the branched DPhPC lipid leaflet is barely affected and remains planar. Above the critical charge imbalance of 10e, the formation of the water channel occurs later than that of pure DPPC lipid bilayers but sooner than that of pure branched DPhPC lipid bilayers. The z coordinates of the phosphorus atoms and the morphology of the biggest water channel are shown in Fig. 12. As can be seen, DPPC lipids in the bottom leaflet rearrange themselves greatly when the water channel forms, with several DPPC lipid headgroups entering the water channel from the bottom leaflet. In contrast, few DPhPC lipid headgroups from the top leaflet move inside the water channel. From Fig. 12b, we find that the water channel in the bottom DPPC leaflet shows a larger curvature than that of the top DPhPC leaflet and the channel in the bottom leaflet is surrounded by more hydrophilic DPPC headgroups.

In another scenario, we mix both linear DPPC and branched DPhPC lipids in each leaflet of the lipid bilayers, as shown in Fig. 1d, and calculate the critical charge imbalance/critical simulation time for formation of the water channel. The results are intermediate between DPPC lipid bilayers and branched DPhPC lipid bilayers, i.e., the water channel forms when the initial charge

imbalance is above 9e. The water channels are toroidal and lined by both DPPC and DPhPC lipids.

## CONCLUSIONS

Using molecular dynamics simulations with a double bilayer setup in a periodic box, we built two water compartments, one with an excess of cations, and the other with an equal excess of anions. The charge imbalance in the two water compartments created a transmembrane potential across the lipid bilayers and resulted in the formation of water channels inside lipid bilayer when the charge imbalance is large enough. We demonstrated that the branched DPhPC lipid bilayers required a higher critical initial transmembrane potential to break down and to allow a water channel to form. When the water channel forms, the linear DPPC lipid heads lined the water channel creating a curved hydrophilic pore surface. The morphologies of the water channels were similar to toroidal pores that form in membranes with pore-forming peptides or proteins. On the other hand, due to the bulkiness of branched DPhPC lipid tails, few DPhPC lipid head groups could rearrange and line the water pores. Instead, cylindrical water channels formed with their morphologies similar to barrel-stave pores. However, unlike peptide-stabilized barrel-stave pores, these barrel-stave water channels were surrounded only by the hydrophobic lipid tails, and were very unstable and shrinked much more quickly when the transmembrane potential decreased. We further showed that even though the formation of a toroidal pore required greater lipid rearrangement, it formed readily, possibly due to the hydrophilic nature of the water channel. In addition, once formed, the hydrophilic toroidal pore also collapsed much more slowly when the potentials were removed than the barrel-stave pores did. Our results might help explain the variations in lipid compositions of various organisms, and help predict the electric fields required to induce electroporation.

## ACKNOWLEDGEMENTS

Inspiration to carry out these simulations was based on helpful discussions with Yvonne Sun. We acknowledge support from NSF under grant NSEC EEC-0425626. Any opinions, findings, and conclusions or recommendations expressed in this material are those of the authors and do not necessarily reflect the views of the National Science Foundation (NSF).

**Electronic Supplementary Information** (ESI) available: Theoretical Models for Critical Electric Field. See DOI: ###/#####.

## REFERENCES


1. J. F. Nagle and S. Tristram-Nagle, *Biochim. Biophys. Acta*, 2000, **1469**, 159–195.
2. S. Bhattacharya and S. Haldar, *Biochim. Biophys. Acta*, 2000, **1467**, 39–53.
3. M. E. Haque, T. J. McIntosh, and B. R. Lentz, *Biochem.*, 2001, **40**, 4340–4348.
4. K. Charalambous, D. Miller, P. Curnow, and P. J. Booth, *BMC Biochem.*, 2008, **9**, 31.
5. N. J. Gibson and M. F. Brown, *Biochem.*, 1993, **32**, 2438–2454.
6. K. J. Hallock, D.-K. Lee, J. Omnaas, H. I. Mosberg, and A. Ramamoorthy, *Biophys. J.*, 2002, **83**, 1004–1013.
7. W. Rawicz, K. C. Olbrich, T. McIntosh, D. Needham, and E. Evans, *Biophys. J.*, 2000, **79**, 328–339.
8. W. T. Heller, K. He, S. J. Ludtke, T. A. Harroun, and H. W. Huang, *Biophys. J.*, 1997, **73**, 239–244.
9. K. Yamauchi, K. Doi, M. Kinoshita, F. Kii, and H. Fukuda, *Biochim. Biophys. Acta*, 1992, **1110**, 171–177.
10. B. Tenchov, E. M. Vescio, G. D. Sprott, M. L. Zeidel, and J. C. Mathai, *J. Biol. Chem.*, 2006, **281**, 10016–10023.
11. E. S. Giotis, D. A. McDowell, I. S. Blair, and B. J. Wilkinson, *Appl. Environ. Microbiol.*, 2007, **73**, 997–1001.
12. M. Andersson, J. Jackman, D. Wilson, P. Jarvoll, V. Alfredsson, G. Okeyo, and R. Duran, *Colloids Surf., B*, 2011, **82**, 550–561.
13. J. C. Mathai, G. D. Sprott, and M. L. Zeidel, *J. Biol. Chem.*, 2001, **276**, 27266–27271.
14. S. Tristram-Nagle, D. J. Kim, N. Akhunzada, N. Kucerka, J. C. Mathai, J. Katsaras, M. Zeidel, and J. F. Nagle, *Chem. Phys. Lipids*, 2010, **163**, 630–637.
15. W. Shinoda, M. Mikami, T. Baba, and M. Hato, *J. Phys. Chem. B*, 2003, **107**, 14030–14035.
16. W. Shinoda, M. Mikami, T. Baba, and M. Hato, *Chem. Phys. Lett.*, 2004, **390**, 35–40.
17. W. Shinoda, M. Mikami, T. Baba, and M. Hato, *J. Phys. Chem. B*, 2004, **108**, 9346–9356.
18. W. Shinoda, K. Shinoda, T. Baba, and M. Mikami, *Biophys. J.*, 2005, **89**, 3195–3202.
19. K. Shinoda, W. Shinoda, and M. Mikami, *Phys. Chem. Chem. Phys.*, 2007, **9**, 643–650.
20. F.-Y. Chen, M.-T. Lee, and H. W. Huang, *Biophys. J.*, 2003, **84**, 3751–3758.
21. F.-Y. Chen, M.-T. Lee, and H. W. Huang, *Biophys. J.*, 2002, **82**, 908–914.
22. C. Hsieh, S. Sue, P. Lyu, and W. Wu, *Biophys. J.*, 1997, **73**, 870–877.
23. D. B. Sawyer, R. E. Koeppe, and O. S. Andersen, *Biophys. J.*, 1990, **57**, 515–523.
24. E. Bárány-Wallje, S. Keller, S. Serowy, S. Geibel, P. Pohl, M. Bienert, and M. Dathe, *Biophys. J.*, 2005, **89**, 2513–2521.
25. L. Yang, T. a Harroun, T. M. Weiss, L. Ding, and H. W. Huang, *Biophys. J.*, 2001, **81**, 1475–1485.
26. K. He, S. J. Ludtke, D. L. Worcester, and H. W. Huang, *Biophys. J.*, 1996, **70**, 2659–2666.
27. L. R. Phillips, C. D. Cole, R. J. Hendershot, M. Cotten, T. A. Cross, and D. D. Busath, *Biophys. J.*, 1999, **77**, 2492–2501.
28. M.-T. Lee, W.-C. Hung, F.-Y. Chen, and H. W. Huang, *Biophys. J.*, 2005, **89**, 4006–4016.
29. J. D. Durrant, D. Caywood, and D. D. Busath, *Biophys. J.*, 2006, **91**, 3230–3241.
30. K. He, S. J. Ludtke, W. T. Heller, and H. W. Huang, *Biophys. J.*, 1996, **71**, 2669–2679.
31. W. T. Heller, K. He, S. J. Ludtke, T. A. Harroun, and H. W. Huang, *Biophys. J.*, 1997, **73**, 239–244.
32. F. Gambale and M. Montal, *Biophys. J.*, 1988, **53**, 771–783.

33. A. M. O'Connell, R. E. Koeppe II, and O. S. Andersen, *Science*, 1990, **250**, 1256–1259.
34. W. C. Hung, F. Y. Chen, and H. W. Huang, *Biochim. Biophys. Acta*, 2000, **1467**, 198–206.
35. H. M. Keizer, B. R. Dorvel, M. Andersson, D. Fine, R. B. Price, J. R. Long, A. Dodabalapur, I. Köper, W. Knoll, P. A. V. Anderson, and R. S. Duran, *ChemBioChem*, 2007, **8**, 1246–1250.
36. G. Valincius, D. J. McGillivray, W. Febo-Ayala, D. J. Vanderah, J. J. Kasianowicz, and M. Lösche, *J. Phys. Chem. B*, 2006, **110**, 10213–10216.
37. K. J. Kwak, G. Valincius, W.-C. Liao, X. Hu, X. Wen, A. Lee, B. Yu, D. J. Vanderah, W. Lu, and L. J. Lee, *Langmuir*, 2010, **26**, 18199–18208.
38. S. Paula, A. G. Volkov, A. N. Van Hoek, T. H. Haines, and D. W. Deamer, *Biophys. J.*, 1996, **70**, 339–348.
39. F. Bordi, C. Cametti, and A. Motta, *J. Phys. Chem. B*, 2000, **104**, 5318–5323.
40. D. W. Deamer and J. Bramhall, *Chem. Phys. Lipids*, 1986, **40**, 167–188.
41. K. A. Brogden, *Nat. Rev. Microbiol.*, 2005, **3**, 238–250.
42. I. Iacovache, M. Bischofberger, and F. G. van der Goot, *Curr. Opin. Struct. Biol.*, 2010, **20**, 241–246.
43. G. Anderluh and J. H. Lakey, *Proteins: Membrane Binding and Pore Formation*, Springer-Verlag, Berlin, 1st edn., 2010.
44. R. A. Böckmann, B. L. de Groot, S. Kakorin, E. Neumann, and H. Grubmüller, *Biophys. J.*, 2008, **95**, 1837–1850.
45. W. F. D. Bennett and D. P. Tieleman, *J. Chem. Theory Comput.*, 2011, **7**, 2981–2988.
46. D. C. Chang, B. M. Chassy, J. A. Saunders, and A. E. Sowers, *Guide to Electroporation and Electrofusion*, Academic, San Diego, CA, 1992.
47. T. Y. Tsong, *Biophys. J.*, 1991, **60**, 297–306.
48. P. Kramar, M. Pavlin, T. Kotnik, and D. Miklavc, *Adv. Planar Lipid Liposomes*, 2008, **6**, 165–226.
49. J. C. Weaver and Y. A. Chizmadzhev, *Bioelectrochem. Bioenerg.*, 1996, **41**, 135–160.
50. D. P. Tieleman, *BMC Biochem.*, 2004, **5**, 1–12.
51. H. Leontiadou, A. E. Mark, and S. J. Marrink, *Biophys. J.*, 2004, **86**, 2156–2164.
52. T. Heimburg, *Biophys. Chem.*, 2010, **150**, 2–22.
53. S. J. Marrink, A. H. de Vries, and D. P. Tieleman, *Biochim. Biophys. Acta*, 2009, **1788**, 149–168.
54. C. A. Jordan, E. Neumann, and A. E. Sowers, in *Electroporation and Electrofusion in Cell Biology*, Plenum Press, New York, 1989, pp. 59–164.
55. A. A. Gurtovenko and I. Vattulainen, *Biophys. J.*, 2007, **92**, 1878–1890.
56. S. K. Kandasamy and R. G. Larson, *J. Chem. Phys.*, 2006, **125**, 074901.
57. J. N. Sachs, P. S. Crozier, and T. B. Woolf, *J. Chem. Phys.*, 2004, **121**, 10847–10851.
58. B. L. Kagan, M. E. Selsted, T. Ganz, and R. I. Lehrer, *Proc. Nat. Acad. Sci.*, 1990, **87**, 210–214.
59. L. Zhang, A. Rozek, and R. E. Hancock, *J. Biol. Chem.*, 2001, **276**, 35714–35722.
60. J. Gallaher, K. Wodzińska, T. Heimburg, and M. Bier, *Phys. Rev. E*, 2010, **81**, 061925.
61. D. P. Tieleman, H. Leontiadou, A. E. Mark, and S.-J. Marrink, *J. Am. Chem. Soc.*, 2003, **125**, 6382–6383.
62. C. Chen, S. W. Smye, M. P. Robinson, and J. A. Evans, *Med. Biol. Eng. Comput.*, 2006, **44**, 5–14.

63. S. Y. Ho and G. S. Mittal, *Crit. Rev. Biotechnol.*, 1996, **16**, 349–362.
64. M. Tarek, *Biophys. J.*, 2005, **88**, 4045–4053.
65. Y. Sun, B. J. Wilkinson, T. Standiford, H. Akinbi, and M. O'Riordan, *J. Bacteriol*, 2012, **194**, 5274–5284.
66. M.-T. Lee, W.-C. Hung, F.-Y. Chen, and H. W. Huang, *Proc. Natl. Acad. Sci. USA*, 2008, **105**, 5087–5092.
67. S. A. Pandit, D. Bostick, and M. L. Berkowitz, *Biophys. J.*, 2003, **84**, 3743–3750.
68. D. Van Der Spoel, E. Lindahl, B. Hess, G. Groenhof, A. E. Mark, and H. J. C. Berendsen, *J. Comput. Chem.*, 2005, **26**, 1701–1718.
69. B. Hess, C. Kutzner, D. van der Spoel, and E. Lindahl, *J. Chem. Theory Comput.*, 2008, **4**, 435–447.
70. A. Kukol, *J. Chem. Theory Comput.*, 2009, **5**, 615–626.
71. J. Domański, P. J. Stansfeld, M. S. P. Sansom, and O. Beckstein, *J. Membr. Biol.*, 2010, **236**, 255–258.
72. S. Leekumjorn and A. K. Sum, *Biochim. Biophys. Acta*, 2007, **1768**, 354–365.
73. J. Wohlert and O. Edholm, *J. Chem. Phys.*, 2006, **125**, 204703.
74. S. J. Marrink, J. Risselada, and A. E. Mark, *Chem. Phys. Lipids*, 2005, **135**, 223–244.
75. E. Lindahl and O. Edholm, *J. Chem. Phys.*, 2001, **115**, 4938.
76. C.-H. Hsieh, S.-C. Sue, P.-C. Lyu, and W.-G. Wu, *Biophys. J.*, 1997, **73**, 870–877.
77. K. Matsuzaki, O. Murase, N. Fujii, and K. Miyajima, *Biochem.*, 1996, **35**, 11361–11368.
78. S. J. Ludtke, K. He, W. T. Heller, T. A. Harroun, L. Yang, and H. W. Huang, *Biochem.*, 1996, **35**, 13723–13728.
79. G. Baumann and P. Mueller, *J. Supramol. Struct.*, 1974, **2**, 538–57.
80. D. P. Tieleman, H. J. Berendsen, and M. S. Sansom, *Biophys. J.*, 2001, **80**, 331–346.
81. R. Glaser, S. Leikin, L. Chernomordik, V. Pastushenko, and A. Sokirko, *Biochim. Biophys. Acta*, 1988, **940**, 275–287.